Desalination and Water Treatment
www.deswater.com
doi: 10.5004/dwt.2020.24872

177 (2020) 71–79
February

Adsorption of triclosan from aqueous solution onto char derived from palm kernel shell

Mutiara Triwiswara[a], Chang-Gu Lee[b], Joon-Kwan Moon[c], Seong-Jik Park[d,*]

[a]*Department of Chemical Engineering, Hankyong National University, 327 Jungang-ro, Anseong, Gyeonggi-do, Republic of Korea, email: triwiswara@gmail.com*
[b]*Department of Environmental and Safety Engineering, Ajou University, 206 World cup-ro, Suwon, Gyeonggi-do, Republic of Korea, email: changgu@ajou.ac.kr (C.-G. Lee)*
[c]*Department of Plant and Environmental Science, Hankyong National University, 327 Jungang-ro, Anseong, Gyeonggi-do, Republic of Korea, email: jkmoon@hknu.ac.kr (J.-K. Moon)*
[d]*Department of Bioresources and Rural System Engineering, Hankyong National University, 327 Jungang-ro, Anseong, Gyeonggi-do, Republic of Korea, Tel. +82-31-670-5131; Fax: +82-31-670-5139; email: parkseongjik@hknu.ac.kr (S.-J. Park)*

Received 9 May 2019; Accepted 8 September 2019

ABSTRACT

Char derived from palm kernel shell (PKS-char) was evaluated as an adsorbent for the removal of triclosan, an antimicrobial agent used in consumer products, from aqueous medium. Despite the low specific surface area of PKS-char, its average pore size is 4.1 nm, which is suitable for the penetration of triclosan into the inner pores. Kinetic experiments showed that with initial triclosan concentrations of 5 and 50 mg L^{-1}, adsorption equilibrium was reached at 6 and 12 h, respectively. The Langmuir model described the equilibrium adsorption of triclosan to PKS-char more suitably than the Freundlich model, indicating that triclosan was adsorbed on PKS-char as a monolayer. The maximum capacity of PKS-char for triclosan adsorption was 88.854 mg g^{-1}, which is higher than that of some commercial activated carbon samples. Triclosan adsorption decreased gradually as the pH increased from 4 to 8, but decreased sharply above pH 8. Thermodynamic experiments showed that the adsorption of triclosan by PKS-char is endothermic and spontaneous under the present experimental conditions. It can be concluded that PKS-char is a low-cost but effective adsorbent for the removal of triclosan from aqueous solutions.

Keywords: Triclosan; Palm kernel shell; Char; Adsorption; Low-cost adsorbent

1. Introduction

Triclosan (5-chloro-2-(2,4-dichlorophenoxy)-phenol) is an antimicrobial agent used in consumer products such as soap, detergent, toothpaste, mouthwash, fabric, deodorant, shampoo, and plastic additives, as well as in other personal care, veterinary, industrial, and household products [1,2]. The concentration in cosmetic products such as toothpastes, mouth rinses, soaps, shampoos, deodorants, and skin care creams is typically in the range of 0.1%–0.3% [3]. Triclosan is preferentially fat-soluble and easily crosses cell membranes. Once inside the cell, triclosan can deteriorate a specific enzyme that many bacteria and fungi need for survival [4].

The widespread use of triclosan provides a number of pathways for it to enter the environment, which raises concerns about its potentially harmful effects on the ecosystem and humans [5]. Triclosan has been reported to be toxic to aquatic organisms and has also been detected in human plasma and milk in Sweden and in human urine in the USA [6]. Moreover, some recent findings indicate that it

* Corresponding author.

blocks bacterial lipid biosynthesis by specifically inhibiting the enzyme enoyl–acyl carrier protein reductase, leading to concerns about the possible development of bacterial resistance to triclosan [4]. Another concern regarding the presence of triclosan in surface water is the formation of more toxic by-products such as dioxin and endocrine disruptor chemicals [1]. In wastewater treatment plants, triclosan is not degraded or is partially degraded, and is therefore, detected in almost every type of aquatic environment, including wastewater treatment effluents, surface water, lakes, and river sediments [5,7].

Various techniques have been applied for the removal of triclosan from water in wastewater treatment systems. Adsorption is regarded as a simple and efficient method for removal of triclosan from aqueous solutions. Adsorption by carbon is considered to be an effective treatment technology for removing small molecular organic compounds such as phenol, due to the high available surface area and the combination of the well-developed pore structure and surface functional group properties of the carbon adsorbents [1,8]. Some commercial powdered activated carbons [1,8], carbon nanotubes [6,9,10], and activated carbon fibers [11] have been reported to be effective for adsorbing triclosan in aqueous solutions. However, the practical application of these materials is uneconomical. This has led to increased interest in the production of activated carbons from low-cost precursors, mainly industrial and agricultural by-products, such as jatropha, date pits, groundnut shells, corncobs, bamboos, rattan sawdust, oil palm fibers, coconut shells, and coconut husk [12–14].

Palm kernel shell (PKS) is an agricultural by-product of palm oil mills and is readily available at low cost, has a high surface area, possess good sorption performance, and is of high quality. Therefore, this material is a suitable raw material for generating activated carbon [13,15]. Recent research has focused on the use of char or activated carbon derived from the PKS for removing pollutants from water, and this sorbent has been proven effective for the adsorption of dyes [12,13,16], mercury [15], and heavy metals [17–19] from aqueous solution. The char derived from biomass is a carbon rich and porous solid, frequently produced via slow pyrolysis under the presence or absence of oxygen [20]. While activated carbons are obtained after an activation step, chars are obtained via thermal treatment but without further activation [21].

To the best of our knowledge, the use of the char derived from PKS (PKS-char) as an adsorbent for triclosan removal has never been studied. This study aims to investigate the utilization of PKS-char for the removal of triclosan from aqueous solution. The physical and chemical properties of PKS-char are investigated. Kinetic and equilibrium adsorption experiments are performed under batch conditions to evaluate the adsorption of triclosan to PKS-char. Further experiments regarding the effect of the solution pH and temperature on the removal of triclosan are also conducted.

2. Materials and methods

2.1. Materials

PKS-char used in this study was provided by Design Factory Co. (Korea). Following the palm oil extraction procedure, PKS-char was produced in a rotary kiln at 350°C for 20 min. After crushing and sieving (0.85–1.18 mm), PKS-char was washed thoroughly with deionized water to remove the impurities and dried in an oven at 105°C for 24 h to remove moisture. The triclosan (≥97%) used for the experiments was supplied by Sigma-Aldrich. Triclosan stock solutions were prepared by dissolving triclosan in high-performance liquid chromatography (HPLC) grade acetonitrile (Burdick & Jackson, US). The stock solutions were stored at 4°C in a dark place to prevent exposure to light, which may cause degradation, and were used within a month of preparation. The sample solutions for all sorption tests were prepared by diluting the stock solution with 20% acetonitrile (prepared with distilled water) to achieve the desired concentration levels. The solubility of triclosan in water and acetonitrile was 0.01 and 1,078.9 g-triclosan/L-solvent at 20°C, respectively [22,23].

2.2. Characterization of PKS-char

The physical and chemical properties of PKS-char were investigated using various methods. A field-emission scanning electron microscope (FE-SEM; S-4700, Hitachi, Japan) with an attached energy dispersive X-ray spectrometer was used to investigate the surface morphology and chemical composition of PKS-char. The specimens of PKS-char before and after adsorption experiments were observed at 1,000× and 10,000× magnification, respectively, at an accelerating voltage of 15 kV. Before imaging, all samples were coated with gold at 30 mA for 120 s to minimize the charging effect. N_2 adsorption–desorption experiments was performed to measure the specific surface area of PKS-char using a surface area analyzer (Quadrasorb SI, Quantachrome Instrument, USA). From the N_2 adsorption–desorption isotherms, the specific surface area was determined via Brunauer–Emmett–Teller analysis. The functional groups on the surface of PKS-char were characterized by attenuated total reflectance-Fourier transform infrared spectroscopy (ATR-FTIR; Nicolet iS10, Thermo Scientific, USA).

2.3. Triclosan removal experiment

Triclosan removal by PKS-char was conducted under batch conditions. Batch experiments were performed by reacting 30 mL of the triclosan solution with 0.2 g of adsorbent in a 50 mL polypropylene conical tube at 25°C and agitation at the rate of 100 rpm, unless otherwise stated. After the reaction, all samples were centrifuged to separate the solution from the PKS-char sample using a centrifuge (Combi 514R, Hanil Science Industrial Co., Ltd., South Korea). The residual triclosan concentration in the sample then was quantified by HPLC. All batch experiments were performed in triplicate.

Kinetic experiments were performed by varying the reaction time from 1 to 24 h with two different initial triclosan concentrations (5 and 50 mg L^{-1}). Equilibrium batch experiments were conducted with different initial triclosan concentrations (1–500 mg L^{-1}), and the samples were analyzed after 24 h. Triclosan adsorption by the adsorbents was evaluated at different pH. In the pH experiments, 0.1 M NaOH and 0.1 M HCl solutions were used to adjust the pH

from 4 to 10. The initial and final pH were measured with a pH meter (Seven-multi S40; Mettler Toledo, Switzerland). The thermodynamic adsorption experiments were also performed by reacting 0.2 g of PKS-char with 30 mL of 50 mg L^{-1} triclosan solution for 24 h at reaction temperatures of 15°C, 25°C, and 35°C.

2.4. Chemical analysis

An HPLC system (LC-20AD Shimadzu, Japan) equipped with a Luna C18(2) column (150 mm × 4.6 mm × 5 μm) and a UV–Vis detector was used to measure the triclosan concentration. A detection wavelength of 280 nm was applied [24]. The mobile phase used for the elution was acetonitrile/trifluoroacetic acid (0.1%) and the flow rate of the eluent through the column was set at 0.8 mL min^{-1}. A sample injection volume of 10 μL was used, and the column temperature was maintained at 30°C throughout the analyses. For quantification purposes, a calibration plot was constructed within the range of experimental concentrations used (coefficient of determination (R^2) greater than 0.99).

2.5. Data analysis

The kinetic data were analyzed using the following pseudo-first-order (Eq. (1)), pseudo-second-order (Eq. (2)), and intra-particle diffusion (Eq. (3)) models [25]:

$$q_t = q_e\left(1 - e^{-k_1 t}\right) \tag{1}$$

$$q_t = \frac{k_2 q_e^2 t}{1 + k_2 q_e t} \tag{2}$$

$$q_t = k_p t^{\frac{1}{2}} + C_i \tag{3}$$

where q_t is the amount of triclosan removed at time t (mg L^{-1}), q_e is the amount of triclosan adsorbed onto PKS-char at equilibrium, k_1 is the pseudo-first-order rate constant (h^{-1}), and k_2 is the pseudo-second-order rate constant (g L^{-1} h^{-1}), k_p (mg g^{-1} $h^{1/2}$), the rate parameter of stage i, was obtained from the slope of the straight line of q_t vs. $t^{1/2}$. C_i, the intercept of stage i, provides an estimate of the thickness of the boundary layer, that is, the larger the intercept, the greater the boundary layer effect. The equilibrium data were analyzed using the following Langmuir (Eq. (4)) and Freundlich (Eq. (5)) isotherm models:

$$q_e = \frac{Q_m K_L C_e}{1 + K_L C_e} \tag{4}$$

$$q_e = K_F C_e^{\frac{1}{n}} \tag{5}$$

where C_e is the concentration of triclosan in the aqueous solution at equilibrium (mg L^{-1}), K_L is the Langmuir constant related to the binding energy (L mg^{-1}), Q_m is the maximum mass of triclosan removed per unit mass of PKS-char (mg g^{-1}), K_F is the distribution coefficient (L g^{-1}), and n is the Freundlich constant. The values of K_L, Q_m, K_F, and n can be determined by fitting the obtained data to the Langmuir and Freundlich models. All parameters of the models were estimated by non-linear regression using Sigma-Plot 10.0 with the Dynamic Fit Wizard function.

The thermodynamic properties of the experimental results were analyzed using the following equations:

$$\Delta G^\circ = \Delta H^\circ - T\Delta S^\circ \tag{6}$$

$$\Delta G^\circ = -RT \ln K_e \tag{7}$$

$$\ln K_e = \frac{\Delta S^\circ}{R} - \frac{\Delta H^\circ}{RT} \tag{8}$$

$$K_e = \frac{\alpha q_e}{C_e} \tag{9}$$

where ΔG° is the change in the Gibb's free energy (kJ mol^{-1}), ΔS° is the change in the entropy (J mol^{-1} K^{-1}), ΔH° is the change in enthalpy (kJ mol^{-1}), R is the gas constant (J mol^{-1} K^{-1}), K_e is the equilibrium constant, and α is the amount of adsorbent (g L^{-1}).

3. Results and discussion

3.1. Characterization of PKS-char

The morphology of the surface of PKS-char was investigated using FE-SEM (Fig. 1). The external surface of PKS-char was dominated by irregular pores with large dimensions and irregular inorganic deposits were also observed (Figs. 1a and b). After adsorption experiments, the smaller pores of PKS-char were observed than before adsorption experiments because of the adsorption of triclosan (Figs. 1c and d). The elemental composition determined by energy dispersive X-ray (EDX) analysis (Table 1) showed that PKS-char was mainly composed of carbon with a small amount of alkaline metal (Na and K) and alkaline earth metal (Mg and Ca) on the surface. After adsorption of triclosan on PKS-char, however, Na, Mg, and Ca were diminished from PKS-char and Cl element, which is the main component of triclosan, was observed.

The Brunauer–Emmett–Teller (BET) specific surface area (S_{BET}) was 16.04 m^2 g^{-1}, with a total pore volume (V_t) of 0.02 cm^3 g^{-1} and average pore diameter (D_p) of 4.1 nm, as determined at −195.8°C. The specific surface area is slightly smaller than that (27.3 m^2 g^{-1}) of chemically modified activated carbon prepared from palm shell [26]. The definition of the pore size originally proposed by Dubinin and now adopted by the International Union of Pure & Applied Chemistry (IUPAC) can be divided into three basic classes: macropores (greater than 50 nm), mesopores (2–50 nm), and micropores (less than 2 nm) [27]. As per the IUPAC classification, the average pore diameter of PKS-char corresponds to mesopores, which is the most suitable size for the adsorption of triclosan. The macropores act as conduits permitting access to the interior part of PKS-char, and hence, to the

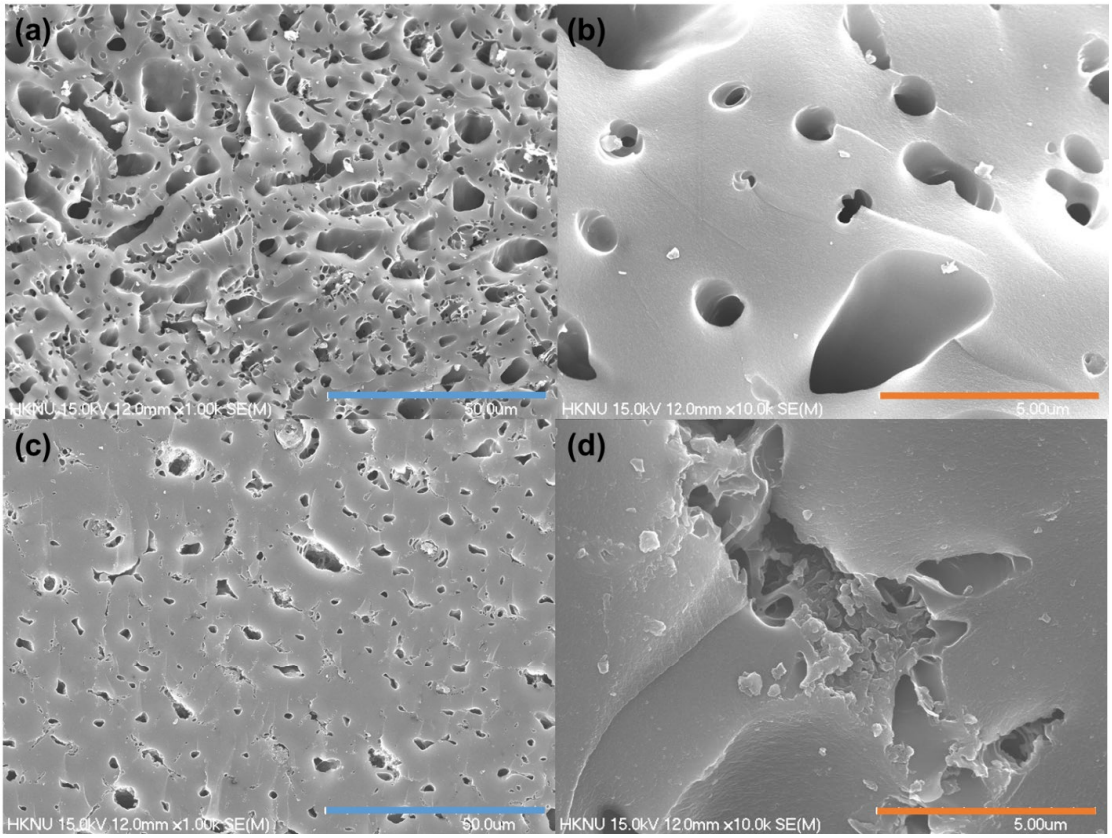

Fig. 1. FE-SEM images of PKS-char before (a, b) and after (c, d) adsorption experiments. The magnifications for (a) and (c) were ×1,000, and for (b) and (d) were ×10,000 (blue bar: 50 μm, orange bar: 5 μm).

Table 1
Elemental composition of PKS-char before and after adsorption experiments obtained from energy dispersive X-ray spectrometry

Element	Before adsorption		After adsorption	
	Weight (%)	Atomic (%)	Weight (%)	Atomic (%)
C	89.78	93.19	94.27	96.07
O	7.29	5.68	4.58	3.50
K	1.46	0.46	0.38	0.12
Si	0.45	0.20	0.42	0.18
Mg	0.38	0.19	–	–
Ca	0.35	0.11	–	–
Na	0.29	0.16	–	–
Cl	–	–	0.35	0.12

mesopores [28]. In contrast with the macropores and mesopores, micropores are too narrow to allow triclosan with dimensions of 1.42 × 0.69 × 0.75 nm [29] to access to the pores. BET analysis also showed that high adsorption of triclosan can be achieved by adsorbents with a pore diameter closer to the molecular size of triclosan via the pore-filling mechanism [30].

The FTIR spectrum of PKS-char in Fig. 2 shows a band at ~3,400 cm^{-1}, associated with the –OH stretching vibration. The prominent band at 1,580 cm^{-1} was assigned to C=C stretching vibration in the aromatic rings. The band observed at 1,170 cm^{-1} was assigned to C–O stretching vibrations. The FTIR band of PKS-char shows no peaks related to N–O, which have been observed in the FTIR profiles some of commercial activated carbons [29]. This result is consistent with the EDX data (Table 1), which did not show the presence of N on the surface of PKS-char.

3.2. Kinetic adsorption of triclosan by PKS-char

The adsorption of triclosan by PKS-char as a function of the contact time is presented in Fig. 3. The solute uptake rate controls the residence time for adsorbate uptake at the solid-solution interface and is, therefore, important for understanding the adsorption kinetics of adsorbates in general [31]. In Fig. 3, the time to reach equilibrium with initial triclosan concentrations of 5 and 50 mg L^{-1} was 6 and 12 h, respectively, indicating that more time is required to reach equilibrium at higher concentrations of triclosan. At the initial stages of the contact period, the adsorption rate was fast, but became slower near the equilibrium time. There were a large number of available vacant surface sites during the initial stage; but after an interval, occupation of the remaining vacant surface sites became difficult because of repulsive forces between the solute molecules on the solid and bulk phases. A similar trend was observed in the adsorption of triclosan on powdered activated carbon and multi-walled carbon nanotubes [1,6]. The high initial adsorption rate

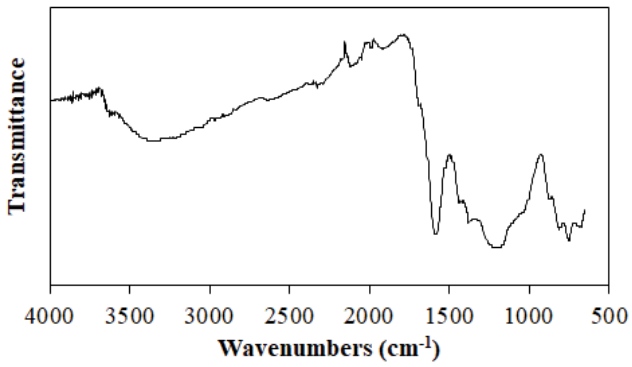

Fig. 2. FTIR-ATR spectrum of PKS-char.

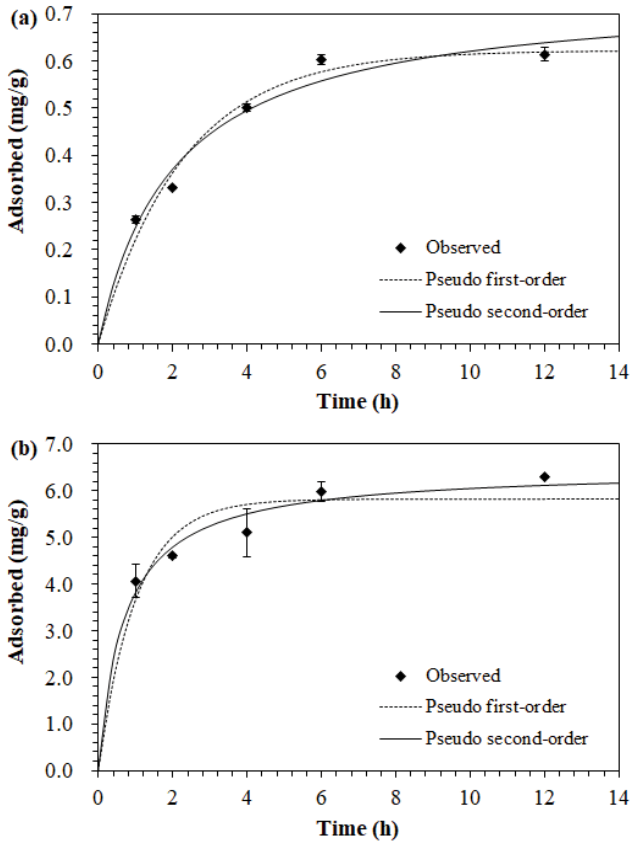

Fig. 3. Experimental kinetic sorption data and model fits for triclosan removal by PKS-char at concentration of (a) 5 mg L^{-1} and (b) 50 mg L^{-1}.

was due to the adsorption of triclosan by the exterior surface of the adsorbent. When saturation was reached at the exterior surface, the triclosan molecules entered the pores of the adsorbent and were adsorbed by the interior surface of the particles [25].

Thus far, various kinetic models have been used to understand the dominant mechanism of the adsorption processes and to predict the behavior over time, because most adsorption transformation processes of various solid phases are time-dependent [32]. To investigate the adsorption kinetics of triclosan, pseudo first-order and pseudo second-order models were employed in this analysis. The amount of triclosan adsorbed by PKS-char at equilibrium based on the pseudo-first-order model was 10%–20% less than that obtained based on the pseudo-second-order model. At higher concentrations of triclosan, the higher R^2 values for the pseudo-second-order model than for the pseudo-first-order model indicate that the observed data obtained at different reaction times are better described by the pseudo-second-order model (Table 2). Therefore, at high triclosan concentration, the rate of adsorption to PKS-char is controlled by chemisorption [33].

As shown in Fig. 4b, the linear line for 5 mg L^{-1} triclosan passed through the origin, but that for 50 mg L^{-1} did not pass through the origin. This deviation from the origin may be due to the difference in the mass transfer rate in the initial and final stages of adsorption [34]. It also indicates that intra-particle diffusion was not the only rate limiting mechanism in the adsorption process at higher triclosan concentrations. This is consistent with the results obtained from the pseudo-second-order model, suggesting that the rate of adsorption at high triclosan concentration (50 mg L^{-1}) is controlled by chemisorption. At 5 mg L^{-1}, however, the results, which were well described by the pseudo-first-order model, indicated diffusion-controlled adsorption. A steeper concentration gradient was achieved at higher concentration, and diffusion of the triclosan molecules onto the surface of PKS-char is more favorable at higher triclosan concentrations. The value of k_p for 50 mg L^{-1} was 1.256 mg g^{-1} $h^{1/2}$, which is greater than that (0.246 mg g^{-1} $h^{1/2}$) for 5 mg L^{-1}, indicating that k_p was larger at higher initial concentrations of triclosan, which may be due to the greater driving force at higher concentration [35].

3.3. Equilibrium adsorption of triclosan to PKS-char

The triclosan adsorption was measured using a fixed amount (0.2 mg) of PKS-char and 12 h contact time to construct the adsorption isotherm. The adsorption isotherm indicates how the adsorbate is distributed between the liquid and the solid phases when the adsorption process reaches the equilibrium state [36]. The amount of triclosan adsorbed on PKS-char as a function of the equilibrium triclosan concentration with the equilibrium model fit is shown in Fig. 5. The parameters related to fitting of the Freundlich and Langmuir models are shown in Table 3.

The values of R^2 demonstrate that the Langmuir model provides a better fit than the Freundlich model for both adsorbents. This result indicates that the binding of triclosan occurs as a monolayer on the surface of PKS-char, and that the uptake occurs on the homogenous surface by monolayer adsorption [15]. As shown in Table 4, the maximum triclosan adsorption capacity, Q_m, for PKS-char was calculated to be 88.854 mg g^{-1}, which is higher than that of commercial activated carbon reported in other studies [1,29,31]. The outstanding adsorption ability of PKS-char might be ascribed to the similarity of its pore size to the dimensions of triclosan and its high hydrophobicity. As described in Section 3.1., the average pore size of PKS-char is similar to the molecular size of triclosan. Because PKS-char is primarily composed of carbon, as shown by the EDX data, the surface of PKS-char should

Table 2
Kinetic model parameters obtained from model fitting of the experimental data for adsorption of triclosan by PKS-char at different reaction times

Initial triclosan concentration (mg L^{-1})	Pseudo-first-order kinetic model parameters			Pseudo-second-order kinetic model parameters			Observed data
	q_e (mg g^{-1})	k_1 (1/h)	R^2	q_e (mg g^{-1})	k_2 (g (mg h)$^{-1}$)	R^2	q_e (mg g^{-1})
5	0.623	0.438	0.967	0.748	0.657	0.956	0.614
50	5.812	0.986	0.739	6.476	0.220	0.905	6.309

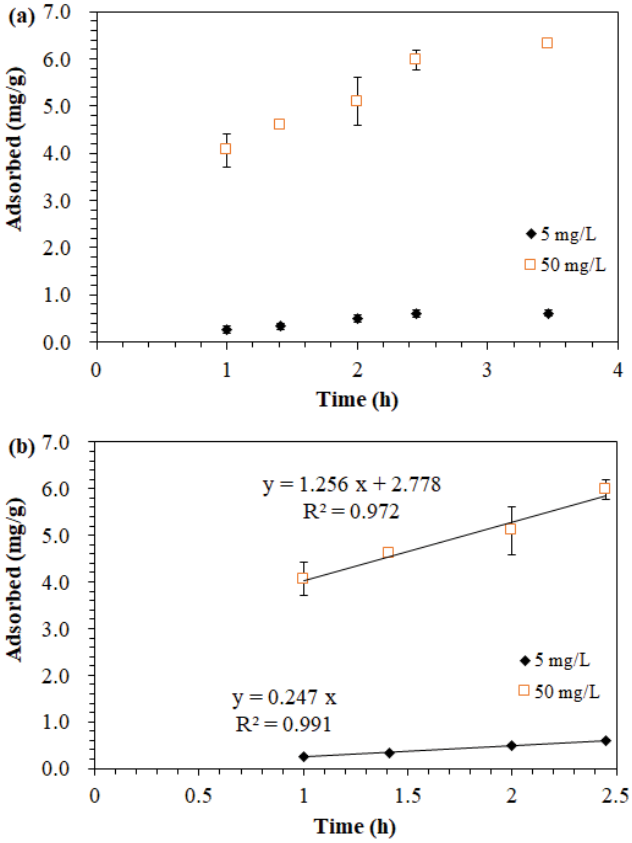

Fig. 4. Intra-particle diffusion model for the adsorption of triclosan to PKS-char: (a) full x-scale and (b) initial step.

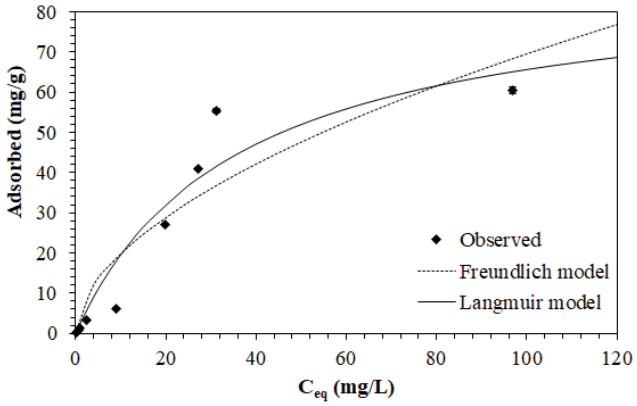

Fig. 5. Experimental equilibrium sorption data and model fits for the adsorption of triclosan to PKS-char.

Table 3
Equilibrium model parameters obtained from model fitting of the experimental data for the adsorption of triclosan to PKS-char

Model	Parameters		R^2
Langmuir	Q_m (mg g^{-1}) 88.854	K_L (L mg^{-1}) 0.028	0.927
Freundlich	K_F ((mg g^{-1}) (L $mg^{-1})^{1/n}$) 5.614	$1/n$ 0.546	0.871

be hydrophobic. Triclosan is also highly hydrophobic [29]; thus, the interaction between PKS-char and triclosan should be favorable. The adsorption capacity of PKS-char is also comparable with that of other synthesized adsorbents. The adsorption capacities of carbon nanotubes, modified activated carbon, and iron oxide and carbon composites are higher than that of PKS-char. The cost of PKS-char is 110 US$/ton (provided by the manufacturer), which is cheaper than commercial activated carbon and much cheaper than synthesized adsorbents that have higher adsorption capacity for triclosan. When the cost of the adsorbents is considered, PKS-char is a competitive adsorbent for the removal of triclosan. Another advantage of using PKS-char is the granular morphology of PKS-char, allowing easy separation from the aqueous medium after treatment, which may be achieved by filtration.

This feature of PKS-char was further confirmed by the value of K_L, which is related to the energy of adsorption between the adsorbent and adsorbate [37]. This property is particularly important for adsorbing triclosan from water at low concentrations, where the adsorption performance at low concentration mainly depends on the adsorption affinity rather than the adsorption capacity [38]. PKS-char has lower affinity than other synthesized adsorbents, but the K_L value of triclosan is similar to that of commercial activated carbon. The $1/n$ value for the Freundlich model was 0.546, which is higher than 0.5, indicating that the binding between triclosan and PKS-char is not strong [39].

3.4. Effect of pH on adsorption

The pH is generally a critical factor influencing the adsorption of pollutants in water because of its ability to affect the surface charge of the sorbent and existing form of the sorbate [31]. Fig. 6 demonstrates the influence of the initial

Table 4
Comparison of maximum monolayer adsorption capacity (Q_m) and adsorption affinity (K_L) of various adsorbents for triclosan

Adsorbents	Q_m (mg g^{-1})	K_L (L mg^{-1})	Specific surface area (m^2 g^{-1})	Reference
Commercial activated carbon	3.5	4.4×10^{-7}	212.56	[31]
Kaolinite	6.03	0.006	2.31	[1]
Montmorillonite	1.79	0.023	34.28	[1]
Cetylpyridinium bromide (CPB) modified zeolites (OZ 2.5)	46.95	0.906	0	[40]
Coconut pulp waste activated carbon	38.91	0.2032	NA[a]	[41]
Carbon nanotubes	40.00	NA	NA	[42]
Charcoal-based activated carbon	67.11	0.023	738.8	[1]
Commercial powdered activated carbon	76.3	1.0	882.63	[29]
PKS-char	88.854	0.028	27.3	This study
Multi-walled carbon nanotubes	160.66	0.03	281	[6]
Magnetic activated carbon	303	0.89	674	[43]
MIL-53(Al)-1 modified activated carbon	488	5.1 ± 1.1	1,270	[44]
γ-Fe_2O_3/carbon composites	892.9	0.69	1,311	[45]

[a]Not available.

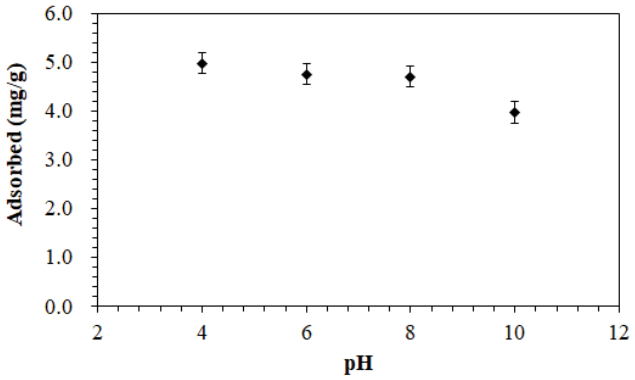

Fig. 6. Effects of solution pH on the adsorption of triclosan to PKS-char.

pH values on the capacity of PKS-char for triclosan adsorption. With an increase in the pH from 4 to 8, the amount of triclosan adsorbed by PKS-char gradually decreased, reaching a value of 4.70 mg g^{-1} at pH 8. With an increase in the pH from 8 to 10, the triclosan adsorption decreased sharply from 4.70 to 3.97 mg g^{-1}. Thus, the removal efficiency decreased from to 62.7% to 52.2% as the pH increased from 8 to 10.

Triclosan mainly exists in the protonated form when the pH of the solution is lower than 8.14 (pKa of triclosan = 8.14). In contrast, the deprotonated form of triclosan predominates in solution when the pH exceeds 8.14, where this species is negatively charged due to the proton loss [1,46]. When adsorption occurs at a pH higher than 8 (pH > pKa), the anionic form of triclosan dominates and the overall surface charge of the adsorbent is negative. Therefore, the adsorption capacity is reduced above pH 8 due to repulsive forces between deprotonated triclosan and the negatively charged adsorbent surface. On the other hand, at acidic pH, even if the net charge of the surface of the adsorbent is negative, the charge of non-dissociated triclosan is neutral. Thus, repulsive electrostatic interactions are minimized and the adsorption capacity is enhanced [1].

The present results are in agreement with reports by other researchers, where it was observed that triclosan adsorption to the adsorbent decreases as the solution pH increases. Similar trends were reported in the adsorption of triclosan to activated carbon [1,31], biochar [7], and multi-walled carbon nanotubes [9], as well as in the adsorption of 2,4,6-trichlorophenol on oil palm empty fruit bunch-based activated carbon [25].

3.5. Thermodynamic adsorption

The thermodynamic concept assumes that in an isolated system where energy cannot be gained or lost, the entropy change is the driving force. The thermodynamic parameters that must be considered to determine the adsorption processes are the changes in the standard enthalpy ($\Delta H°$), standard entropy ($\Delta S°$), and standard free energy ($\Delta G°$) due to transfer of a unit mole of solute from solution onto the solid–liquid interface. The values of $\Delta H°$ and $\Delta S°$ can, respectively, be calculated from the slope and intercept of the van't Hoff plot of ln K_c vs. $1/T$ (Fig. 7). The calculated values of $\Delta H°$, $\Delta S°$, and $\Delta G°$ and for adsorption of triclosan on PKS-char are listed in Table 5.

The positive $\Delta H°$ value indicates that the adsorption process is endothermic. This finding is consistent with the results obtained earlier [25], where the triclosan uptake increased with increasing solution temperature. A decrease in the viscosity of the solution due to temperature increase might lead to increased rate of diffusion of the adsorbate molecules across the external boundary layer and in the internal pores of the adsorbent particles; this phenomenon might explain the endothermic nature of the adsorption [25]. An increase in the adsorption with increasing temperature might also be due to enhanced mobility of the adsorbate

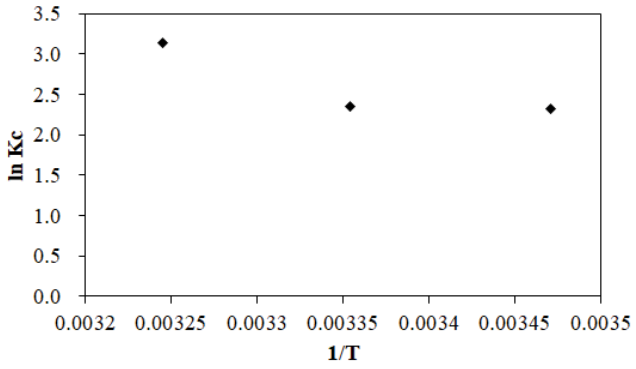

Fig. 7. Thermodynamic analysis of the adsorption of triclosan to PKS-char.

Table 5
Thermodynamic parameters for the adsorption of triclosan on PKS-char

Temperature (K)	ΔH (kJ/mol)	ΔS (kJ/mol)	ΔG (kJ/mol)
288.15			–5.48
298.15	7.32	0.044	–5.93
308.15			–6.33

molecules [47]. It is reported that the kind of interaction can be classified by the magnitude of $\Delta H°$ [48]. The $\Delta H°$ ranges for van der Waals interactions, electrostatic interaction, and chemisorption are usually <20, 20–80, and 80–450 kJ/mol, respectively [6,48]. In this study the magnitude of $\Delta H°$ (7.32 kJ/mol) suggested the existence of van der Waals interactions between triclosan and PKS-char.

The positive $\Delta S°$ indicates the affinity of the adsorbent for triclosan and the increasing randomness at the solid–solution interface with some structural changes in the adsorbate and adsorbent during the adsorption process, whereas the negative $\Delta G°$ indicates the spontaneous nature of the adsorption process in the evaluated temperature range.

4. Conclusion

The feasibility of PKS-char for the removal of triclosan from aqueous solution was investigated under batch conditions. PKS-char is mainly composed of carbon (~90%), and based on its average pore size, it is classified as mesoporous material. Kinetic adsorption experiments showed that the adsorption of triclosan at low concentrations was controlled by diffusion, whereas chemisorption controlled the rate of triclosan adsorption at high concentrations. The Langmuir model was more suitable for describing triclosan adsorption than the Freundlich model, indicating that triclosan was adsorbed onto PKS-char via monolayer adsorption. The maximum adsorption capacity of PKS-char was 88.854 mg g^{-1}, which is superior to that of commercially available activated carbon but lower than that of other synthesized adsorbents reported in the literature. The capacity of PKS-char for triclosan adsorption was higher under acidic rather than alkaline conditions; the adsorption is endothermic and spontaneous in nature. This study demonstrates that PKS-char can be considered as an effective adsorbent for triclosan removal from wastewater because of its low cost and high adsorption capacity.

Acknowledgments

This work was supported by Korea Institute of Planning and Evaluation for Technology in Food, Agriculture, Forestry and Fisheries (IPET) through Advanced Production Technology Development Program, funded by Ministry of Agriculture, Food and Rural Affairs (MAFRA) (Grant No. 317017-03).

Symbols

α	—	Amount of adsorbent, g L^{-1}
C_e	—	Concentration of triclosan in the aqueous solution at equilibrium, mg L^{-1}
$\Delta G°$	—	Change in the Gibb's free energy, kJ mol^{-1}
$\Delta H°$	—	Change in enthalpy, kJ mol^{-1}
$\Delta S°$	—	Change in the entropy, J mol^{-1} K^{-1}
k_p	—	Rate parameter of stage i, mg/g $h^{1/2}$
K_L	—	Langmuir constant related to the binding energy, L mg^{-1}
K_F	—	Distribution coefficient, L g^{-1}
K_e	—	Equilibrium constant
k_2	—	Pseudo-second-order rate constant, g L^{-1} h^{-1}
k_1	—	Pseudo-first-order rate constant, h^{-1}
n	—	Freundlich constant
q_t	—	Amount of triclosan removed at time t, mg L^{-1}
q_e	—	Amount of triclosan adsorbed onto PKS-char at equilibrium
Q_m	—	Maximum mass of triclosan removed per unit mass of PKS-char, mg g^{-1}
R	—	Gas constant, J mol^{-1} K^{-1}

References

[1] S.K. Behera, S.-Y. Oh, H.-S. Park, Sorption of triclosan onto activated carbon, kaolinite and montmorillonite: effects of pH, ionic strength, and humic acid, J. Hazard. Mater., 179 (2010) 684–691.
[2] A.B. Dann, A. Hontela, Triclosan: environmental exposure, toxicity and mechanisms of action, J. Appl. Toxicol., 31 (2011) 285–311.
[3] D. Sabaliunas, S.F. Webb, A. Hauk, M. Jacob, W.S. Eckhoff, Environmental fate of triclosan in the river Aire Basin, UK, Water Res., 37 (2003) 3145–3154.
[4] G.-G. Ying, R.S. Kookana, Triclosan in wastewaters and biosolids from Australian wastewater treatment plants, Environ. Int., 33 (2007) 199–205.
[5] J. López-Morales, O. Perales-Pérez, F. Román-Velázquez, Sorption of triclosan onto Tyre Crumb Rubber, Adsorpt. Sci. Technol., 30 (2012) 831–845.
[6] S. Zhou, Y. Shao, N. Gao, J. Deng, C. Tan, Equilibrium, kinetic, and thermodynamic studies on the adsorption of triclosan onto multi-walled carbon nanotubes, Clean Soil Air Water, 41 (2013) 539–547.
[7] Y. Tong, B.K. Mayer, P.J. McNamara, Triclosan adsorption using wastewater biosolids-derived biochar, Environ. Sci. Water Res. Technol., 2 (2016) 761–768.
[8] S.F. Fang, P. Pendleton, A. Badalyan, Effects of surface functional groups of activated carbon on adsorption of triclosan from aqueous solution, Int. J. Environ. Technol. Manage., 10 (2009) 36–45.

[9] X. Hu, Z. Cheng, Z. Sun, H. Zhu, Adsorption of diclofenac and triclosan in aqueous solution by purified multi-walled carbon nanotubes, Pol. J. Environ. Stud., 26 (2017) 87–95.
[10] H.H. Cho, H. Huang, K. Schwab, Effects of solution chemistry on the adsorption of ibuprofen and triclosan onto carbon nanotubes. Langmuir, 27 (2011) 12960–12967.
[11] L. Xin, Y. Sun, J. Feng, J. Wang, D. He, Degradation of triclosan in aqueous solution by dielectric barrier discharge plasma combined with activated carbon fibers, Chemosphere, 144 (2016) 855–863.
[12] I.A.W. Tan, A.L. Ahmad, B.H. Hameed, Enhancement of basic dye adsorption uptake from aqueous solutions using chemically modified oil palm shell activated carbon, Colloids Surf., A, 318 (2008) 88–96.
[13] T.S.Y. Choong, T.N. Wong, T.G. Chuah, A. Idris, Film-pore-concentration-dependent surface diffusion model for the adsorption of dye onto palm kernel shell activated carbon, J. Colloid Interface Sci., 301 (2006) 436–440.
[14] A.R. Hidayu, N. Muda, Preparation and characterization of impregnated activated carbon from palm kernel shell and coconut shell for CO_2 capture, Procedia Eng., 148 (2016) 106–113.
[15] A.A. Ismaiel, M.K. Aroua, R. Yusoff, Palm shell activated carbon impregnated with task-specific ionic-liquids as a novel adsorbent for the removal of mercury from contaminated water, Chem. Eng. J., 225 (2013) 306–314.
[16] A. Jumasiah, T.G. Chuah, J. Gimbon, T.S.Y. Choong, I. Azni, Adsorption of basic dye onto palm kernel shell activated carbon: sorption equilibrium and kinetics studies, Desalination, 186 (2005) 57–64.
[17] S.M. Nomanbhay, K. Palanisamy, Removal of heavy metal from industrial wastewater using chitosan coated oil palm shell charcoal, Electron. J. Biotechnol., 8 (2005) 43–53.
[18] G. Issabayeva, M.K. Aroua, N.M.N. Sulaiman, Removal of lead from aqueous solutions on palm shell activated carbon, Bioresour. Technol., 97 (2006) 2350–2355.
[19] H.L.H. Chong, P.S. Chia, M.N. Ahmad, The adsorption of heavy metal by Bornean oil palm shell and its potential application as constructed wetland media, Bioresour. Technol., 130 (2013) 181–186.
[20] X.J. Lee, L.Y. Lee, S. Gan, S. Thangalazhy-Gopakumar, H.K. Ng, Biochar potential evaluation of palm oil wastes through slow pyrolysis: thermochemical characterization and pyrolytic kinetic studies, Bioresour. Technol., 236 (2017) 155–163.
[21] J. Bedia, M. Peñas-Garzón, A. Gómez-Avilés, J. Rodriguez, C.A. Belver, Review on the synthesis and characterization of biomass-derived carbons for adsorption of emerging contaminants from water, C J. Carbon Res., 4 (2018) 63.
[22] D.R. Delgado, A.R. Holguin, F. Martinez, Solution thermodynamics of triclosan and triclocarban in some volatile organic solvents, Vitae, 19 (2012) 79–92.
[23] D.G. Lee, Removal of a synthetic broad-spectrum antimicrobial agent, triclosan, in wastewater treatment systems: a short review, Environ. Eng. Res., 20 (2015) 111–120.
[24] A.A. Sharipova, S.B. Aidarova, N.E. Bekturganova, A. Tleuova, M. Schenderlein, O. Lygina, S. Lyubchik, R. Miller, Triclosan as model system for the adsorption on recycled adsorbent materials, Colloids Surf., A, 505 (2016) 193–196.
[25] I.A.W. Tan, A.L. Ahmad, B.H. Hameed, Adsorption isotherms, kinetics, thermodynamics and desorption studies of 2,4,6-trichlorophenol on oil palm empty fruit bunch-based activated carbon, J. Hazard. Mater., 164 (2009) 473–482.
[26] H. Thangappan, A. Valiya Parambathu, S. Joseph, Surface characterization and methylene blue adsorption studies on a mesoporous adsorbent from chemically modified *Areca triandra* palm shell, Desal. Wat. Treat., 57 (2016) 21118–21129.
[27] B.K. Pradhan, N.K. Sandle, Effect of different oxidizing agent treatments on the surface properties of activated carbons, Carbon, 37 (1999) 1323–1332.
[28] O.W. Achaw, A Study of the Porosity of Activated Carbons Using the Scanning Electron Microscope, In V. Kazmiruk, Ed., Scanning Electron Microscopy, IntechOpen, 2012.
[29] H. Kaur, A. Bansiwal, G. Hippargi, G.R. Pophali, Effect of hydrophobicity of pharmaceuticals and personal care products for adsorption on activated carbon: adsorption isotherms, kinetics and mechanism, Environ. Sci. Pollut. Res., 25 (2018) 20473–20485.
[30] G. Newcombe, M. Drikas, R. Hayes, Influence of characterised natural organic material on activated carbon adsorption: II. Effect on pore volume distribution and adsorption of 2-methylisoborneol, Water Res., 31 (1997) 1065–1073.
[31] F. Wang, X. Lu, W. Peng, Y. Deng, T. Zhang, Y. Hu, X.-y. Li, Sorption behavior of bisphenol A and triclosan by graphene: comparison with activated carbon, ACS Omega, 2 (2017) 5378–5384.
[32] Y. Chen, F. Wang, L. Duan, H. Yang, J. Gao, Tetracycline adsorption onto rice husk ash, an agricultural waste: its kinetic and thermodynamic studies, J. Mol. Liq., 222 (2016) 487–494.
[33] E. Bulut, M. Özacar, İ.A. Şengil, Equilibrium and kinetic data and process design for adsorption of Congo Red onto bentonite, J. Hazard. Mater., 154 (2008) 613–622.
[34] K. Mohanty, D. Das, M.N. Biswas, Adsorption of phenol from aqueous solutions using activated carbons prepared from *Tectona grandis* sawdust by $ZnCl_2$ activation, Chem. Eng. J., 115 (2005) 121–131.
[35] A. Özer, G. Dursun, Removal of methylene blue from aqueous solution by dehydrated wheat bran carbon, J. Hazard. Mater., 146 (2007) 262–269.
[36] R. Baccar, M. Sarrà, J. Bouzid, M. Feki, P. Blánquez, Removal of pharmaceutical compounds by activated carbon prepared from agricultural by-product, Chem. Eng. J., 211 (2012) 310–317.
[37] X. Guo, F. Chen, Removal of arsenic by bead cellulose loaded with iron oxyhydroxide from groundwater, Environ. Sci. Technol., 39 (2005) 6808–6818.
[38] C. Shan, Z. Ma, M. Tong, Efficient removal of trace antimony (III) through adsorption by hematite modified magnetic nanoparticles, J. Hazard. Mater., 268 (2014) 229–236.
[39] R.S. Summers, D.R.U. Knappe, V.L. Snoeyink, Adsorption of Organic Compounds by Activated Carbon, In: Water quality and Treatment: A Handbook on Drinking Water, 6th Edition, Edited by J. K. Edzwald, McGraw-Hill, 2011.
[40] C. Lei, Y. Hu, M. He, Adsorption characteristics of triclosan from aqueous solution onto cetylpyridinium bromide (CPB) modified zeolites, Chem. Eng. J., 219 (2013) 361–370.
[41] N.K.E.M. Khori, T. Hadibarata, M.S. Elshikh, A.A. Al-Ghamdi, Salmiati, Z. Yusop, Triclosan removal by adsorption using activated carbon derived from waste biomass: isotherms and kinetic studies, J. Chin. Chem. Soc., 65 (2018) 951–959.
[42] X. Hu, N. Zhao, J. Wei, Adsorption of triclosan on carbonnanotubes, Chin. J. Environ. Eng., 8 (2009) 1462–1464.
[43] Y. Liu, X. Zhu, F. Qian, S. Zhang, J. Chen, Magnetic activated carbon prepared from rice straw-derived hydrochar for triclosan removal, RSC Adv., 4 (2014) 63620–63626.
[44] R. Dou, J. Zhang, Y. Chen, S. Feng, High efficiency removal of triclosan by structure-directing agent modified mesoporous MIL-53(Al), Environ. Sci. Pollut. Res., 24 (2017) 8778–8789.
[45] X. Zhu, Y. Liu, G. Luo, F. Qian, S. Zhang, J. Chen, Facile fabrication of magnetic carbon composites from hydrochar via simultaneous activation and magnetization for triclosan adsorption, Environ. Sci. Technol., 48 (2014) 5840–5848.
[46] J. Xu, J. Niu, X. Zhang, J. Liu, G. Cao, X. Kong, Sorption of triclosan on electrospun fibrous membranes: effects of pH and dissolved organic matter, Emerg. Contam., 1 (2015) 25–32.
[47] S. Senthilkumaar, P. Kalaamani, K. Porkodi, P.R. Varadarajan, C.V. Subburaam, Adsorption of dissolved Reactive red dye from aqueous phase onto activated carbon prepared from agricultural waste, Bioresour. Technol., 97 (2006) 1618–1625.
[48] F.M. Machado, C.P. Bergmann, T.H. Fernandes, E.C. Lima, B. Royer, T. Calvete, S.B. Fagan, Adsorption of reactive Red M-2BE dye from water solutions by multi-walled carbon nanotubes and activated carbon, J. Hazard. Mater., 192 (2011) 1122–1131.